

1 Towards a Pixel TPC part I: construction and test of a  
2 32-chip GridPix detector

3 M. van Beuzekom<sup>a</sup>, Y. Bilevych<sup>b</sup>, K. Desch<sup>b</sup>, S. van Doesburg<sup>a</sup>,  
4 H. van der Graaf<sup>a</sup>, F. Hartjes<sup>a</sup>, J. Kaminski<sup>b</sup>, P.M. Kluit<sup>a</sup>,  
5 N. van der Kolk<sup>a</sup>, C. Ligtenberg<sup>a</sup>, G. Raven<sup>a</sup>, J. Timmermans<sup>a</sup>

6 <sup>a</sup>*Nikhef, Science Park 105, 1098 XG Amsterdam, The Netherlands*

7 <sup>b</sup>*Physikalisches Institut, University of Bonn, Nussallee 12, 53115 Bonn,*  
8 *Germany*

---

9 **Abstract**

10 A Time Projection Chamber (TPC) module with 32 GridPix chips was con-  
11 structed and the performance was measured using data taken in a testbeam  
12 at DESY in 2021. The GridPix chips each consist of a Timepix3 ASIC  
13 (TPX3) with an integrated amplification grid and have a high efficiency of  
14 about 85% to detect single ionisation electrons. In the testbeam setup, the  
15 module was placed in between two sets of Mimosas26 silicon detector planes  
16 that provided external high precision tracking and the whole detector setup  
17 was slid into the PCMAG magnet at DESY. The TPC could be operated  
18 reliably and used a 93.6/5.0/1.4 gas mixture (by volume) of Ar/iC<sub>4</sub>H<sub>10</sub>/CO<sub>2</sub>  
19 with a small amount of oxygen and water vapour. The analysed data were  
20 taken at electron beam momenta of 5 and 6 GeV/c and at magnetic fields of  
21 0 and 1 T.

22 The result for the transverse diffusion coefficient  $D_T$  is  $(287.2 \pm 0.5)$   
23  $\mu\text{m}/\sqrt{\text{cm}}$  at  $B = 0$  T and  $D_T$   $(120.3 \pm 0.5) \mu\text{m}/\sqrt{\text{cm}}$  at  $B = 1$  T. The  
24 longitudinal diffusion coefficient  $D_L$  is measured to be  $(251 \pm 14) \mu\text{m}/\sqrt{\text{cm}}$

---

\*Corresponding author, Telephone: +31 20 592 2000  
*Preprint submitted to Nuclear Instruments and Methods A*  
Email address: s01@nikhef.nl (P.M. Kluit)

25 at  $B = 0$  T and  $(224 \pm 14) \mu\text{m}/\sqrt{\text{cm}}$  at  $B = 1$  T. Results for the tracking  
26 systematical uncertainties in  $xy$  (pixel plane) were measured to be smaller  
27 than  $13 \mu\text{m}$  with and without magnetic field. The tracking systematical  
28 uncertainties in  $z$  (drift direction) were smaller than  $15 \mu\text{m}$  ( $B = 0$  T) and  
29  $20 \mu\text{m}$  ( $B = 1$  T).

30 *Keywords:*

31 Micromegas, gaseous pixel detector, micro-pattern gaseous detector,  
32 Timepix, GridPix, pixel time projection chamber

---

## 33 1. Introduction

34 Earlier publications on a single chip [1] and four chip (quad) GridPix de-  
35 tectors [2] showed the potential of the GridPix technology and the large range  
36 of applications for these devices [3]. In particular, it was demonstrated that  
37 single ionisation electrons can be detected with high efficiency and accuracy,  
38 allowing excellent 3D track position measurements and particle identification  
39 based on the number of electrons and clusters.

40 As a next step towards a Pixel Time Projection Chamber for a future  
41 collider experiment [4], [5], a module consisting of 32 GridPix chips based on  
42 the TPX3 chip was constructed.

43 A GridPix detector consists of a CMOS pixel TPX3 chip [6] with inte-  
44 grated amplification grid added by photo-lithographic - Micro-electromechanical  
45 Systems (MEMS) - post-processing techniques. The TPX3 chip can be op-  
46 erated with a low threshold of  $515 e^-$ , and has a low equivalent noise charge  
47 of about  $70 e^-$ . The GridPix single chip and quad detectors have a very  
48 fine granularity of  $55 \times 55 \mu\text{m}^2$  with  $256 \times 256$  pixels per chip. The device has

49 a high efficiency of about 85% - discussed in this paper - to detect single  
50 ionisation electrons.

51 Based on the experience gained with these detectors a 32 GridPix detector  
52 module - consisting of 8 quad detectors - was built. A drift box defining the  
53 electric field and gas envelop was constructed. A read out system for up to  
54 128 chips with 4 multiplexers read out by one Speedy Pixel Detector Readout  
55 (SPIDR) board [7] [8] was designed. After a series of tests using the laser  
56 setup [9] and cosmics in the laboratory at Nikhef, the detector was taken to  
57 DESY for a two week testbeam campaign.

58 At DESY, the 32-chip detector was placed in between two sets of Mi-  
59 mosa26 silicon detector planes and mounted on a movable stage. The whole  
60 detector setup was slid into the centre of the PCMAG magnet at DESY. A  
61 beam trigger was provided by scintillator counters. The data reported here  
62 were taken at different stage positions and electron beam momenta of 5 and  
63 6 GeV/c and at magnetic fields of 0 and 1 T. The performance of the 32  
64 GridPix detector module was measured using these data sets.

65 In this paper, part I of the results will be presented with the main focus  
66 on the detector spatial resolution and tracking performance. A second follow  
67 up paper will discuss the  $dE/dx$  (or  $dN/dx$ ) and other results.

## 68 **2. The 32-GridPix detector module**

69 A 32 GridPix detector module was built using the quad detector module  
70 [2] as a basic building block. The quad module consists of four GridPix chips  
71 and is optimised for a high fraction of sensitive area of 68.9%. The external  
72 dimensions are 39.60 mm  $\times$  28.38 mm. The four chips which are mounted

73 on a cooled base plate (COCA), are connected with wire bonds to a common  
74 central 6 mm wide PCB. A 10 mm wide guard electrode is placed over the  
75 wire bonds 1.1 mm above the aluminium grids, in order to prevent field  
76 distortions of the electric drift field. The guard electrode is the main inactive  
77 area, and its dimensions are set by the space required for the wire bonds.  
78 On the back side of the quad module, the PCB is connected to a low voltage  
79 regulator. The aluminium grids of the GridPix detectors are connected by  
80 80  $\mu\text{m}$  insulated copper wires to a high voltage (HV) filtering board. The  
81 quad module consumes about 8 W of power of which 2 W is used in the LV  
82 regulator.

83 Eight quad modules were embedded in a box, resulting in a GridPix  
84 detector module with a total of 32 chips. A schematic 3-dimensional drawing  
85 of the detector is shown in Figure 1. A schematic drawing of the quad  
86 detectors in the module is shown in Figure 2, where also the beam direction  
87 is indicated.

88 The internal dimensions of the box are 79 mm along the  $x$ -axis, 192 mm  
89 along the  $y$ -axis, and 53 mm along the  $z$ -axis (drift direction), and it has a  
90 maximum drift length (distance between cathode and read out anode) of 40  
91 mm. The drift field is shaped by a series of parallel CuBe field wires of 75  
92  $\mu\text{m}$  diameter with a wire pitch of 2 mm. Guard strips are located on all of  
93 the four sides of the active area. In addition, six guard wires - shown with  
94 dashed lines (one colored red) in Figure 2 - are suspended over the boundaries  
95 of the chips, to minimise distortions of the electric drift field. The wires are  
96 located at a distance of 1.15 mm from the grid planes, and their potential is  
97 set to the drift potential at this drift distance. The box has two 50  $\mu\text{m}$  thick

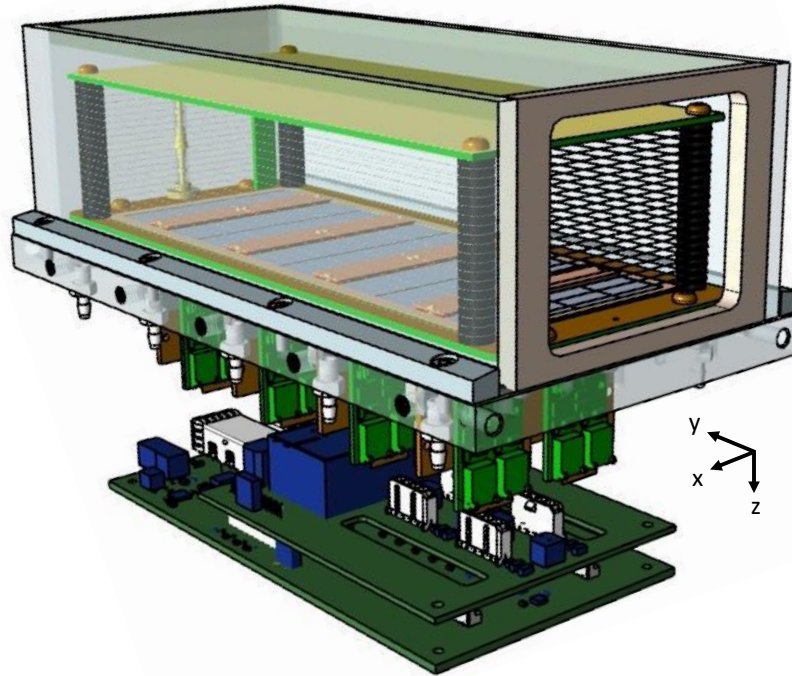


Figure 1: Schematic 3-dimensional rendering of the 32-GridPix module detector for illustration purposes.

98 Kapton windows to allow the beam to pass with minimal multiple scattering.

99 The gas volume of 780 ml is continuously flushed at a rate of  $\sim 50$  ml/min  
100 (about 4 volumes/hour) with premixed T2K TPC gas. This gas is a mixture  
101 consisting of 95% Ar, 3%  $\text{CF}_4$ , and 2%  $\text{iC}_4\text{H}_{10}$  suitable for large TPCs because  
102 of the low transverse diffusion in a magnetic field and the high drift velocity.

103 The data acquisition system of the quad module was adopted to allow for  
104 reading out multiple quad detectors. A multiplexer card was developed that  
105 handles four quad detectors or 16 chips and combines the TPX3 data into  
106 one data stream. For the 32 GridPix module two multiplexers are connected  
107 to a SPIDR board that controls the chips and read out process. The read

108 out speed per chip is 160 Mbps and for the multiplexer 2.56 Gbps this cor-  
 109 responds to a maximum rate of 21 MHits/s. For each pixel the precise Time  
 110 of Arrival (ToA) using a 640 MHz TDC and the time over threshold (ToT)  
 111 are measured.

### 112 3. Experimental setup

113 In preparation of the two weeks DESY testbeam campaign, a support  
 114 frame was designed to move the 32-chip GridPix detector module in the  
 115 plane perpendicular to the beam by a remotely controlled stage such that  
 116 the whole detector volume could be probed. The module was mounted upside  
 117 down with respect to Figure 1 to allow access to the electronics from above.

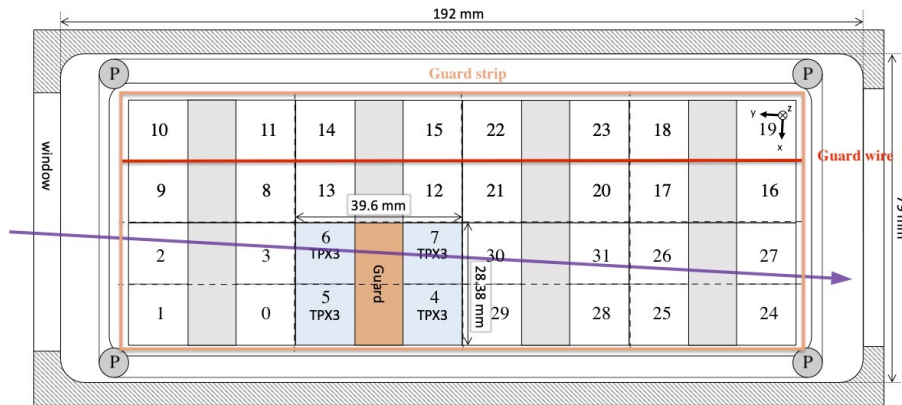


Figure 2: Schematic drawing of the 32-GridPix module detector with one example quad as viewed from the top of the quad detectors. The chips are numbered and the beam direction is shown in purple. A guard electrode of a quad detector is shown in orange. The four surrounding guard strips are shown -not to scale- in orange. Six guard wires - are shown with dashed lines (one colored red) and the pillars of the drift box are shown as circles with a P in the centre.

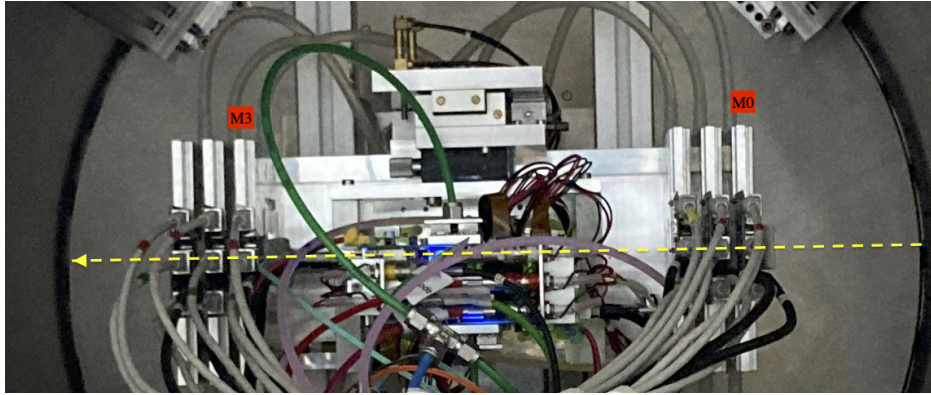


Figure 3: Photo of the detector setup - side view - at the centre of the PCMAG magnet (the circular contour). The Mimosa26 planes M0 and M3 are indicated in red as well as the beam direction (yellow).

118 The support frame also held three Mimosa26 silicon detector planes [10] -  
119 with an active area of  $(21.2 \text{ mm} \times 10.6 \text{ mm})$  - placed in front of the detector  
120 and three Mimosa26 planes behind the detector. At DESY, the Mimosa26  
121 silicon detector planes were provided by the testbeam coordinators. The  
122 whole detector setup was slid towards the centre of the PCMAG magnet  
123 at the DESY II testbeam facility [10]. A beam trigger was provided by a  
124 double scintillator counter coincidence. The data were taken at different  
125 stage positions to cover the whole sensitive TPC volume. Runs with electron  
126 beam momenta of 5 and 6 GeV/c and at magnetic fields of 0 and 1 T were  
127 analysed.

128 A photograph of the detector setup in the PCMAG magnet is shown in  
129 Figure 3. The stage positions of the TPC module with respect to the beam  
130 and the Mimosa26 planes can be adjusted.

131 The experimental and environmental parameters such as temperature,

132 pressure, gas flow and oxygen content were measured and logged by a Win-  
 133 dows operated slow control system. The experimental parameters are sum-  
 134 marised in Table 1. The chips were cooled by circulating Glycol through  
 135 the cooling channels in the module carrier plate. The cooling blocks of the  
 136 multiplexers were further cooled by blowing pressurised air on them.

Table 1: Overview of the experimental parameters. The ranges indicate the variation over the data taking period

Number of analysed runs at $B=0$ (1) T	6 (8)
Run duration	10-90 minutes
Number of triggers per run	3-100 k
$E_{\text{drift}}$	280 V/cm
$V_{\text{grid}}$	340 V
Threshold	550 $e^-$
Gas temperature	303.3-306.6 K
Pressure	1011 – 1023 mbar
Oxygen concentration	240 - 620 ppm
Water vapour concentration	2000 - 7000 ppm

137 The data was produced in four main data streams: one stream produced  
 138 by the Mimosa26 telescope, two data streams by the two Timepix multiplex-  
 139 ers and one trigger stream. The double scintillator coincidence provided a  
 140 trigger signal to the Trigger Logic Unit (TLU) [11] that sends a signal to the  
 141 telescope read out and the trigger SPIDR. The data acquisition systems of  
 142 the telescope and trigger SPIDR injected a time stamp into their respective  
 143 data streams. Hits from the Mimosa26 planes were collected with a sliding  
 144 window of  $-115 \mu\text{s}$  to  $230 \mu\text{s}$  around the trigger time. The data acquisition



145 of the multiplexer and the trigger SPIDR were synchronised at the start of  
146 the run. By comparing the time stamps in these streams, telescope tracks  
147 and TPC tracks could be matched. Unfortunately, the SPIDR trigger had  
148 - due to a cabling mistake at the output of the TLU - a common 25 ns flat  
149 time jitter.

150 After a short data taking period one of the chips (nr 11) developed a  
151 short circuit and the HV on the grid of the chip was disconnected. After the  
152 testbeam data taking period the module was repaired in the clean room in  
153 Bonn.

## 154 4. Analysis

### 155 4.1. Telescope track reconstruction procedure

156 The data of the telescope is decoded and analysed using the Corryvreckan  
157 software package [12]. The track model used for fitting was the General  
158 Broken Lines (GBL) software [14]. The code was extended and optimised to  
159 fit curved broken lines for the data with magnetic field. The telescope planes  
160 were iteratively aligned using the standard alignment software provided by  
161 the package. The single point Mimosas26 resolution is  $4 \mu\text{m}$  in  $x$  and  $6 \mu\text{m}$   
162 in  $z$  (drift direction) [10].

163 Telescope tracks were selected were required to have hits in at least 5 out  
164 of the 6 planes and a total  $\chi^2$  of better than 25 per degree of freedom. The  
165 uncertainties on the telescope track prediction in the middle of the GridPix  
166 detector module are dominated by multiple scattering. The amount of mul-  
167 tiple scattering was estimated by comparing the predictions from the two  
168 telescope arms for 6 GeV/c tracks at  $B = 0$  T. The expected uncertainty in

169  $x$  and  $z$  is  $26 \mu\text{m}$  on average.

#### 170 4.2. TPC Track reconstruction procedure

171 GridPx hits are selected requiring a minimum time over threshold ToT  
172 of  $0.15 \mu\text{s}$ . The drift time is defined as the measured time of arrival minus  
173 the trigger time recorded in the trigger SPIDR data stream minus a fixed  $t_0$   
174 (the drift time at zero drift). The drift time was corrected for time walk [2]  
175 using the measured time over threshold (ToT in units of  $\mu\text{s}$ ) and the formula  
176 (1):

$$\delta t = \frac{18.6(ns \mu s)}{\text{ToT} + 0.1577(\mu s)}. \quad (1)$$

177 Furthermore, small time shift corrections - with an odd-even and a  $16 \times$  pixels  
178 structure - coming from the TPX3 clock distribution were extracted from the  
179 data and applied.

180 The  $z$  drift coordinate was calculated as the product of the drift time  
181 and the drift velocity. This implies that  $z_{\text{drift}} = -z$  as defined in Figure 1.  
182 GridPix hits outside an acceptance window of  $30 \text{ mm}$  wide in  $x$  and  $15 \text{ mm}$   
183 wide in  $z$  were not used in the track finding and reconstruction. Based on  
184 a Hough transform an estimate of the TPC track position and angles in the  
185 middle of the module (at  $y = 1436$  pixels) were obtained. This estimate was  
186 used to collect the hits around the TPC track and fit the track parameters.  
187 For this fit a linear (for  $B = 0 \text{ T}$  data) or a quadratic track (for  $B = 1 \text{ T}$  data)  
188 model was used. In the fit, the expected uncertainties per hit  $\sigma_{xy}$  and  $\sigma_z$  were  
189 used. The expected uncertainties were derived using the parametrisations  
190 discussed in section 5. The fit was iterated three times to reject outlier hits

Table 2: Table with track/event selection cuts

Track/Event Selection

$$|x_{\text{TPC}} - x_{\text{telescope}}| < 0.3 \text{ mm}$$

$$|z_{\text{TPC}} - z_{\text{telescope}}| < 2 \text{ mm}$$

$$|dx/dy_{\text{TPC}} - dx/dy_{\text{telescope}}| < 4 \text{ mrad}$$

$$|dz/dy_{\text{TPC}} - dz/dy_{\text{telescope}}| < 2 \text{ mrad}$$

191 at respectively 10, 5 and 2.5 sigma. A TPC track was required to have a  
 192 least 100 hits in each multiplexer. At least 25% of the total number of hits  
 193 should be on track and the  $\chi^2$  per degree of freedom had to be less than 3 in  
 194  $xy$  and  $zy$ . All track parameters were expressed at a plane in the middle of  
 195 the TPC module.

196 The calibration and alignment of the detector was done using high quality  
 197 tracks for which the track selections are summarised in table 2.

198 The drift velocity was calibrated per run by fitting a linear function to  
 199 the  $z$  (predicted from the telescope track at the measured TPC hit position)  
 200 versus the measured drift time in the TPC. For the  $B = 0$  T runs it varies  
 201 between 61.6 and 63.0  $\mu\text{m}/\text{ns}$ . For the  $B = 1$  T runs it is between 57.2 and  
 202 59.1  $\mu\text{m}/\text{ns}$ . The variation comes mainly from the changes in the relative  
 203 humidity of the gas volume due to small leaks.

204 The individual TPX3 chips were iteratively aligned fitting a shift in  $x$   
 205 ( $z$  *drift*) and two slopes  $dx(z \text{ drift})/drow(\text{column})$ . The alignment was  
 206 done per run, because the detector was moved in  $x$  and/or  $z$  for each run.  
 207 The fitted slopes were also corrected for small shifts and rotations (3D) in  
 208 the nominal chip position.

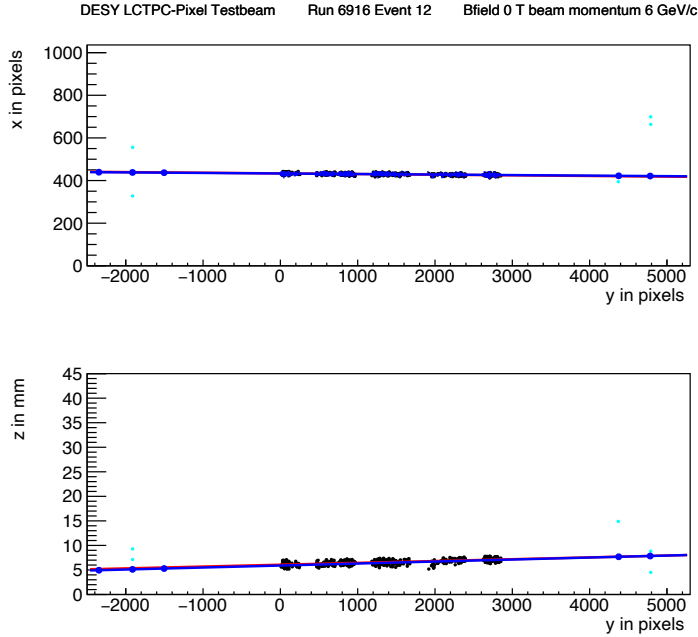


Figure 4: An event display for run 6916 without  $B$  field, with in total 1293 TPC hits (black dots) in the precision plane  $(x, y)$  and drift plane  $(z \text{ drift}, y)$ . The fitted TPC track (red line) with 1130 hits on track and the telescope track (blue line) with 5 Mimosa26 planes (blue hits) on track are shown. In green the off track Mimosa26 hits are shown.

209     An example event from run 6916 without  $B$  field with a TPC and a  
 210 telescope track is shown in Figure 4. The TPC is located between  $y = 0$  and  
 211 2872 pixels. Three Mimosa26 planes are located at  $y < -1000$  and three at  
 212  $y > 4000$  pixels.

## 213 5. Hit resolutions

214     The track residual in  $xy$  is the closest point of the the hit at the center  
 215 of the pixel to track in the  $xy$  plane. The residual in  $z$  is calculated at this  
 216 point of closest approach. The single electron hit resolutions in  $xy$  and  $z$  will

217 be extracted from the track residuals. In order to study the single electron  
 218 resolution for the data with and without magnetic field, additional selections  
 219 on the telescope and TPC tracks were applied. Firstly, due to the trigger  
 220 time jitter of 25 ns (corresponding to 1.5 mm drift), the prediction of the  
 221 telescope track in  $z$  must be used as the reference for  $z$ . Secondly, the  $z$  hits  
 222 of the TPC track were fitted to correct for the common time shift and the  
 223  $z$  residuals were calculated with respect to the fitted TPC track. In the  $xy$   
 224 plane the residuals of TPC hits with respect to the telescope track were used  
 225 to extract the single electron resolution in  $xy$ . For the resolution studies,  
 226 runs at three different  $z$  stage positions of the TPC were selected where the  
 227 beam gave hits in the central chips. The data of 14 central chips (9, 12, 21,  
 228 20, 17, 16, 2, 3, 6, 7, 30, 31, 26 and 27) were used. Two chips (8 and 13)  
 229 were left out because of the E field deformations caused by the short circuit  
 230 in chip 11.

### 231 5.1. Hit resolutions in the pixel plane

232 The residual of the hits in the pixel plane ( $xy$ ) was measured as a function  
 233 of the predicted drift position ( $z_{\text{drift}}$ ). Tracks were selected that crossed the  
 234 fiducial region defined by the central core of the beam. Hits were removed  
 235 in a region of 20 pixels near the chip edges in  $x$ . The spread on the residual  
 236 in  $xy$  for an ionisation electron is given by:

$$\sigma_{xy}^2 = \sigma_{\text{track}}^2 + \frac{d_{\text{pixel}}^2}{12} + D_T^2(z_{\text{drift}} - z_0), \quad (2)$$

237 where  $\sigma_{\text{track}}$  is the uncertainty from the track prediction,  $d_{\text{pixel}}$  is the pixel  
 238 pitch size,  $z_0$  is the position of the grid, and  $D_T$  is the transverse diffusion  
 239 coefficient. The last two terms correspond to the single electron detector

240 resolution (squared). The resolution at zero drift distance  $d_{\text{pixel}}/\sqrt{12}$  was  
 241 fixed to  $15.9 \mu\text{m}$  and  $\sigma_{\text{track}}$  to  $30 \mu\text{m}$  for  $B = 0 \text{ T}$  and  $42 \mu\text{m}$  for  $B =$   
 242  $1 \text{ T}$  data. The uncertainty on the track prediction was measured and is  
 243 larger than the Mimosa plane resolution because of multiple scattering in  
 244 the sensors and in the entrance and exit windows.

245 The expression (2) - leaving  $z_0$  and  $D_T$  as free parameters - is fitted  
 246 to the  $B = 0 \text{ T}$  data shown in Figure 5. The fit gives a transverse diffusion  
 247 coefficient  $D_T$  of  $(287.2 \pm 0.5) \mu\text{m}/\sqrt{\text{cm}}$ . The measured value is in agreement  
 248 with the value of  $287 \mu\text{m}/\sqrt{\text{cm}} \pm 4\%$  predicted by the gas simulation software  
 249 Magboltz 11.9 [15]. The values of the diffusion coefficients depend on the  
 250 humidity that was not precisely measured during the testbeam. The humidity  
 251 strongly affects the drift velocity. Therefore the drift velocity prediction from  
 252 Magboltz was used to determine the water content per run and predictions  
 253 for the diffusion coefficients could be obtained.

254 A fit to the  $B = 1 \text{ T}$  data, also shown in Figure 5, gives a transverse  
 255 diffusion coefficient  $D_T$  of  $(120.3 \pm 0.5) \mu\text{m}/\sqrt{\text{cm}}$ . The measured value is in  
 256 agreement with the value of  $119 \mu\text{m}/\sqrt{\text{cm}} \pm 2\%$  predicted by Magboltz.

## 257 5.2. Hit resolution in the drift plane

258 The spread on the residuals in  $z$  of the ionisation electrons  $\sigma_z$  is given by:

$$\sigma_z^2 = \sigma_{\text{track}}^2 + \sigma_{z_0}^2 + D_L^2(z_{\text{drift}} - z_0), \quad (3)$$

259 where  $\sigma_{\text{track}}$  is the expected track uncertainty,  $\sigma_{z_0}$  the detector resolution at  
 260 zero drift distance and  $D_L$  the longitudinal diffusion constant. The last two  
 261 terms in the equation correspond to the single electron detector resolution  
 262 (squared). Only tracks crossing the fiducial region - defined by the central

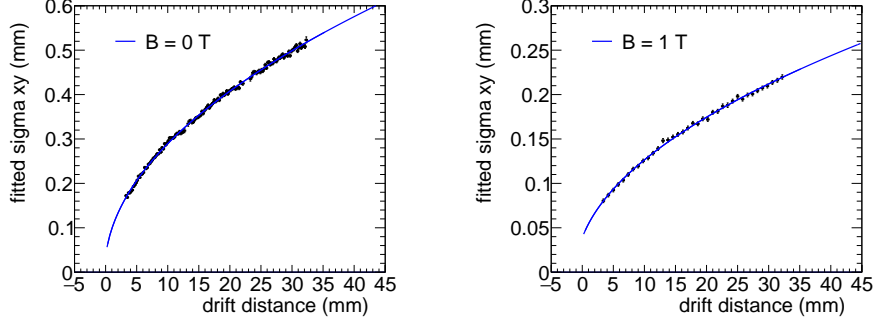


Figure 5: Measured spread on the residuals in the pixel plane (black points) fitted with equation (2) (blue line).

263 core of the beam - were accepted and hits with a ToT value above  $0.6 \mu\text{s}$   
 264 were selected. Because of the time jitter, the fitted TPC track is used for the  
 265 drift residuals. For  $z_{\text{drift}}$  the telescope prediction at the hit was used. The  
 266 expected uncertainty on TPC track prediction is propagated and amounts to  
 267  $50 \mu\text{m}$  at  $z = z_0$ . The systematic uncertainty on  $\sigma_{\text{track}}$  is estimated to  
 268 be  $25 \mu\text{m}$ .

269 The expression (3) - leaving  $\sigma_{z_0}$  and  $D_L$  as free parameters - is fitted  
 270 to the  $B = 0 \text{ T}$  data shown in Figure 6. The value of  $z_0$  was fixed to the  
 271 result of the fit in the  $xy$  plane. The value of  $\sigma_{z_0}$  was measured to be  $129$   
 272  $\mu\text{m}$ . The longitudinal diffusion coefficient  $D_L$  was determined to be  $(251$   
 273  $\pm 1 \text{ (stat)} \pm 14 \text{ (sys)}) \mu\text{m}/\sqrt{\text{cm}}$ , which is higher than the expected value  
 274  $236 \pm 3 \mu\text{m}/\sqrt{\text{cm}}$  from a Magboltz calculation [15]. The quoted systematic  
 275 uncertainty on  $D_L$  is rather large and obtained from a fit using  $\sigma_{\text{track}} = 25$   
 276  $\mu\text{m}$ .

277 A fit to the  $B = 1 \text{ T}$  data shown in Figure 6 gives a longitudinal diffusion  
 278 coefficient  $D_L$  of  $(224 \pm 2 \text{ (stat)} \pm 14 \text{ (sys)}) \mu\text{m}/\sqrt{\text{cm}}$ . The measured value

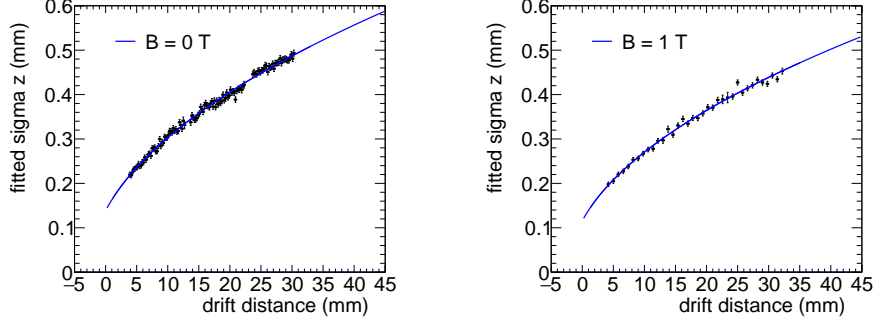


Figure 6: Measured spread on the residuals in the drift plane for hits with a ToT above  $0.60 \mu\text{s}$ . The data are fitted with the expression of equation (3).

279 is lower than the value of  $(245 \pm 4) \mu\text{m}/\sqrt{\text{cm}}$  predicted by Magboltz. The  
 280 fitted value of  $\sigma_{z0}$  was  $114 \mu\text{m}$ .

### 281 5.3. Deformations in the pixel and drift plane

282 It is important to measure possible deformations in the pixel ( $xy$ ) and  
 283 drift ( $z$ ) plane to quantify the tracking precision. For the construction of  
 284 a large Pixel TPC, deformations in the pixel plane deformation should be  
 285 controlled to better than typically  $20 \mu\text{m}$  because these affect the momentum  
 286 resolution. The mean residuals in the pixel and drift planes are shown in  
 287 Figure 7 for the  $B = 0 \text{ T}$  data set using a large set of runs to cover the whole  
 288 module. The residuals were calculated with respect to the telescope track  
 289 prediction. Because of limited statistics, bins were grouped into  $8 \times 16$  pixels.  
 290 Bins with less than 100 hits are left out and residuals larger (smaller) than  
 291  $+(-)100 \mu\text{m}$  are shown in red (blue).

292 A few critical areas can be observed in Figure 7: the region around chip 11  
 293 is affected (chips 14, 8 and 13), because the grid of chip 11 was disconnected.



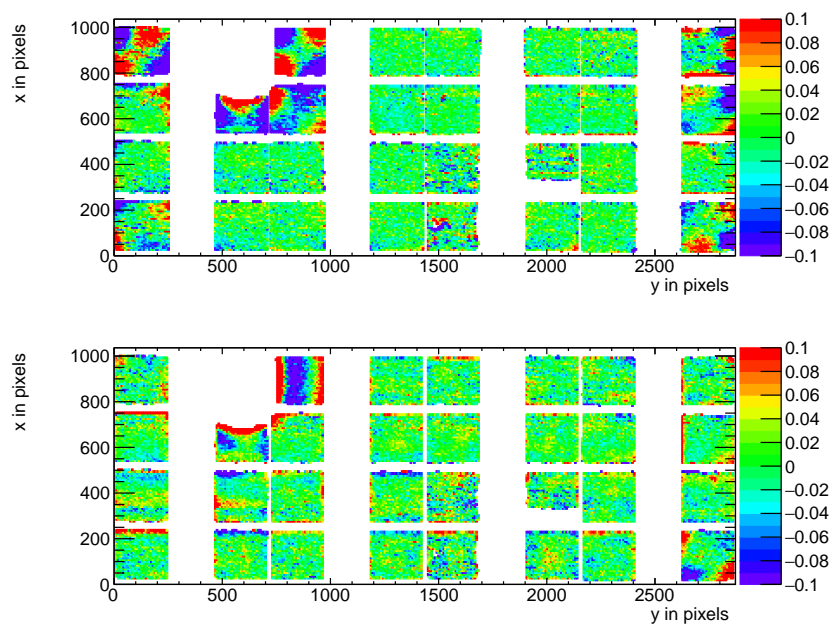


Figure 7: Mean residuals (color coded in mm) in the pixel (top) and drift (bottom) plane for  $B = 0$  T data at the expected hit position.

294 Deformations are present at the four corners of the drift box (chips 1, 10, 19  
295 and 24) and close to the upper corner edge (chip 16) of the drift box. These  
296 come from inhomogenities in the drift field near the supporting pillars, the  
297 field wires are too close to the chip to provide a constant electric field. It  
298 was concluded that for the deformation studies the hits of these nine chips  
299 have to be removed. The track fit was redone leaving these hits out of the fit,  
300 such that they could not bias and affect the results. Note that a bias in the  
301 mean residual at the edge of the chips is expected to be present for an ideal  
302 detector because of the finite coverage and the diffusion in the drift process.

303 In order to reduce the statistical fluctuations and quantify the tracking  
304 precision, the module was regrouped in  $(4 \times 256) \times 256$  pixel planes put side  
305 by side on the horizontal axis, as shown in Figure 8. E.g. the selected chips  
306 from the upper left and bottom left quad detectors are superimposed into  
307 the 0-256 ( $x$ ) and 0-256 ( $y$ ) plane. Bins have a size of  $16 \times 16$  pixels and bins  
308 with less than 1000 entries are not shown. Due to the presence of the dike,  
309 pixels at the edge of the chip became covered and inefficient. Therefore, the  
310 region of 5 pixels in  $y$  near the edge of the chip was removed. For the drift  
311 coordinate studies, a region of 10 pixels near the edge of the chip in  $x$  and  
312  $y$  was removed. The total number of measurements (bins) in  $xy$  is 895 and  
313 in  $z$  892. One can observe that in the module plane no clear systematic  
314 deviations are present and conclude that the guard wire voltages were on  
315 average well tuned. Note that in the quad detector module we had no guard  
316 wires and deformation corrections had to be applied [2]. The r.m.s. of the  
317 distribution of the measured mean residual over the surface in the pixel plane  
318 is  $11 \mu\text{m}$  and in the drift plane  $15 \mu\text{m}$ . Similarly, regrouping the module in

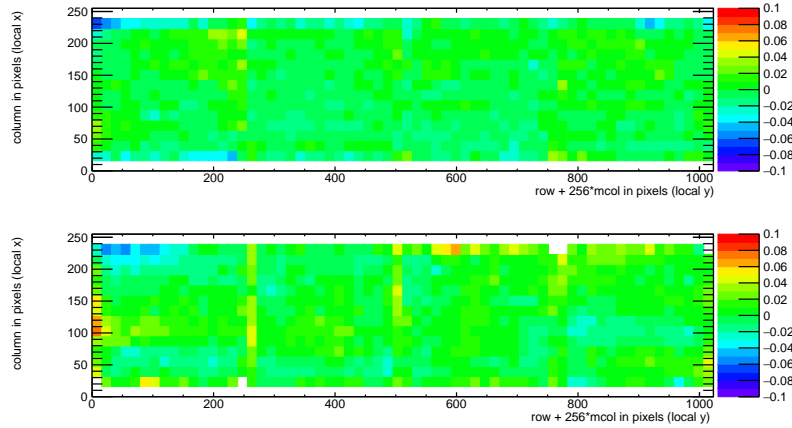


Figure 8: Mean residuals (color coded in mm) in the pixel (top) and drift plane (bottom) for  $B = 0$  T data at the expected hit position.

319  $256 \times (4 \times 256)$  pixels put them side by side on the vertical axis, yielded a  
 320 r.m.s. in the pixel plane of  $13 \mu\text{m}$  and  $13 \mu\text{m}$  in the drift coordinate. The  
 321 expected statistical error - obtained by propagating the uncertainties on the  
 322 residuals - in  $xy$  is  $4 \mu\text{m}$  and in  $z$   $5 \mu\text{m}$ .

323 In the  $B = 1$  T data set, the electrons will drift mainly along the magnetic  
 324 field lines. Deformations are in that case due to e.g. the non-alignment of the  
 325 electric and magnetic field, giving  $E \times B$  effects. Unfortunately, the statistics  
 326 of the telescope tracks that have a matched TPC track was insufficient and  
 327 did not cover the full TPC module plane. Therefore the larger statistics of  
 328 matched and unmatched TPC tracks was used. TPC tracks were required  
 329 to pass angular selection cuts ( $dx/dy$  between  $-40$  and  $-20$  mrad and  $dz/dy$   
 330 between  $0$  and  $14$  mrad) and a momentum cut ( $p > 2$  GeV/c and  $q < 0$ ).

331 The mean residuals in the pixel and drift planes are shown in Figure 9 for  
 332 the  $B = 1$  T data set using a large set of runs to cover the whole module. The

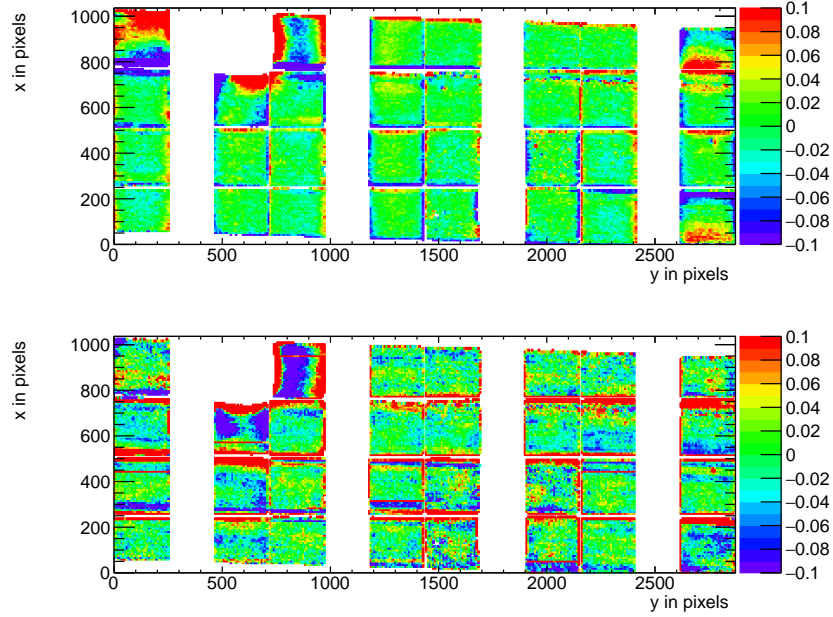


Figure 9: Mean residuals (color coded in mm) in the pixel and drift plane for  $B = 1$  T data at the expected hit position.

333 (biased) residuals were calculated with respect to the TPC track prediction.  
 334 Because of limited statistics, bins were grouped into  $16 \times 16$  pixels. Bins with  
 335 less than 100 hits are left out and residuals larger (smaller) than  $+(-)100 \mu\text{m}$   
 336 are shown in red (blue).

337 In Figure 9 the critical areas discussed above - around chip 11, the four  
 338 corner chips and chip 16 in the upper corner edge - can be clearly observed.  
 339 For the deformation studies, the hits of these nine chips were removed. The  
 340 TPC track fit was redone leaving these hits out of the fit, thus that they could  
 341 not bias and affect the results. The TPC plane is well covered, although one  
 342 can observe that due to the angle of the beam in the  $xy$  plane the chips in  
 343 the upper right and lower left corners are not fully covered.

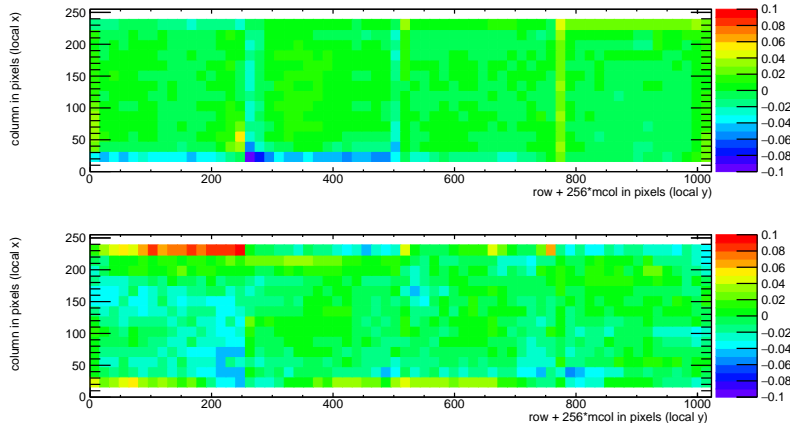


Figure 10: Mean residuals (color coded in mm) in the pixel and drift plane for  $B = 1\text{T}$  data at the expected hit position.

344 In order to reduce the statistical fluctuations and quantify the tracking  
 345 precision, the module was again regrouped in  $(4 \times 256) \times 256$  pixels as de-  
 346 scribed above, as shown in Figure 10. Bins have a size of  $16 \times 16$  pixels and  
 347 bins with less than 1000 entries are not shown. Similar to the no-field defor-  
 348 mations studies, acceptance cuts had to be applied. The region of 16 pixels  
 349 in  $y$  near the edge of the chips was removed. For the drift coordinate studies,  
 350 in addition a region of 10 pixels in  $x$  near the edge of the chip was removed.  
 351 The total number of measurements (bins) in  $xy$  is 896 and in  $z$  896. One can  
 352 observe that in the module plane no clear systematic deviations are present.  
 353 The r.m.s. of the distribution of the measured mean residual over the surface  
 354 in the pixel plane is  $13 \mu\text{m}$  and in the drift plane  $19 \mu\text{m}$ . Similarly, regroup-  
 355 ing the module in  $256 \times (4 \times 256)$ , yielded a r.m.s. in the pixel plane of  $11 \mu\text{m}$   
 356 and  $20 \mu\text{m}$  in the drift coordinate. The expected statistical error in  $xy$  is 2  
 357  $\mu\text{m}$  and in  $z$   $3 \mu\text{m}$ .

358 In summary, the deformations studies for the  $B = 0$  and 1 T data demon-  
359 strate that the systematical uncertainties in  $xy$  are smaller than  $13 \mu\text{m}$  with  
360 and without magnetic field. The systematical uncertainties in  $z$  were smaller  
361 than  $15 \mu\text{m}$  ( $B = 0$  T) and  $20 \mu\text{m}$  ( $B = 1$  T).

#### 362 5.4. Tracking resolution

363 A selected TPC track in the  $B = 0$  T data has on average 1000 hits. The  
364 tracking precision in the middle of the TPC (at  $y = 1436$  pixels) was derived  
365 on a track-by-track basis, by propagating the pixel TPC hit uncertainties. It  
366 was found to be on average  $9 \mu\text{m}$  in the precision plane and  $13 \mu\text{m}$  in  $z$ . The  
367 angular resolution in  $dx/dy$  was on average 0.19 mrad and for  $dz/dy$  0.25  
368 mrad. It is clear that the position resolution in the TPC in the precision  
369 and drift coordinates is impressive for a track length of (only) 158 mm.  
370 The values are smaller than the uncertainty on the track prediction from  
371 the silicon telescope of  $26 \mu\text{m}$  in  $x$  and  $z$  on average that is dominated by  
372 multiple scattering.

### 373 6. Single electron efficiency

374 The distribution of the number of TPC track hits per chip - without  
375 requiring a matched telescope track - are shown in Figure 11 for the data  
376 without magnetic field and for the  $B = 1$  T data. For the  $B = 0$  T data, the  
377 central chips 2,6,7,9,16,17,26 and 27 were selected. For the  $B = 1$  T data,  
378 the same chips plus chips 12,13,20 and 21 were selected.

379 The mean number of hits is measured to be 124 and 89 in the  $B = 0$  T  
380 and 1 T data sets respectively. The most probable values are respectively  
381 87 and 64. Note that the  $B = 0$  T data have a much larger Landau-like

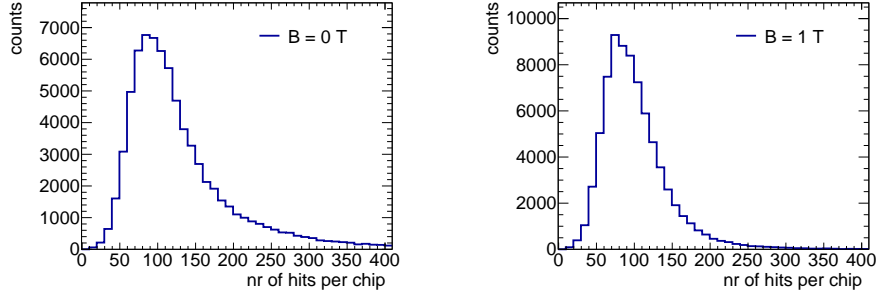


Figure 11: Distribution of the number of TPC track hits per chip for  $B = 0$  T (left)  $B = 1$  T data.

382 tail than the 1 T data. Also the fluctuations in the core of the distribution  
 383 are larger. The mean time over threshold (ToT) is  $0.68 \mu\text{s}$  for the  $B = 0$  T  
 384 and  $0.86 \mu\text{s}$  at a  $B = 1$  T data. A typical ToT distribution can be found  
 385 in Figure 5.5 of ref.[4]. The time over threshold is related to the deposited  
 386 charge. This means that the deposited charge per pixel is smaller for the 0  
 387 T data. The most probable value for the total deposited charge is similar for  
 388 both data sets. A possible explanation for this behavior is that because of  
 389 the reduced transverse diffusion in the  $B = 1$  T data, the possibility of two  
 390 primary electrons ending up in a single grid hole is higher. The mean number  
 391 of hits is in agreement with the prediction of 106 electron-ion pairs for a 5  
 392 and 6 GeV/c electron at  $B = 0$  T for the T2K gas by [13], crossing 236 pixels  
 393 or 12.98 mm and a detector running at 85% single electron efficiency. The  
 394 measured single electron efficiency at this working point is in agreement with  
 395 the efficiency vs mean time over threshold curve that was measured using a  
 396 Fe source [4].

397 **7. Conclusion and outlook**

398 A TPC module with 32 GridPix chips was constructed and the perfor-  
399 mance was measured using data taken in a testbeam at DESY in 2021. The  
400 TPC could be operated reliably and used a 93.6/5.0/1.4 gas mixture (by vol-  
401 ume) of Ar/iC<sub>4</sub>H<sub>10</sub>/CO<sub>2</sub> with a small amount of oxygen and water vapour.  
402 The analysed data were taken at electron beam momenta of 5 and 6 GeV/c  
403 and at magnetic fields of 0 and 1 T.

404 The result for the transverse diffusion coefficient  $D_T$  is  $(287.2 \pm 0.5)$   
405  $\mu\text{m}/\sqrt{\text{cm}}$  at  $B = 0$  T and  $D_T$  is  $(120.3 \pm 0.5) \mu\text{m}/\sqrt{\text{cm}}$  at  $B = 1$  T. The  
406 longitudinal diffusion coefficient  $D_L$  is measured to be  $(251 \pm 14) \mu\text{m}/\sqrt{\text{cm}}$   
407 at  $B = 0$  T and  $(224 \pm 14) \mu\text{m}/\sqrt{\text{cm}}$  at  $B = 1$  T. Results for the tracking  
408 systematical uncertainties in  $xy$  were measured to be smaller than 13  $\mu\text{m}$   
409 with and without magnetic field. The tracking systematical uncertainties in  
410  $z$  were smaller than 15  $\mu\text{m}$  ( $B = 0$  T) and 20  $\mu\text{m}$  ( $B = 1$  T).

411 The mean number of hits is in agreement with the predictions of [13] and  
412 a detector running at 85% single electron efficiency.

413 Not all data were analysed and users are welcome to study them using  
414 the data sets on available on the Grid.

415 The GridPix detector will be further tested and developed in view of a  
416 TPC that will be installed in a heavy ion experiment at the EIC or other  
417 future colliders. A follow up paper is in preparation on the measured  $dE/dx$   
418 or  $dN/dx$  resolution and other performance topics.



419 **Acknowledgements**

420 This research was funded by the Netherlands Organisation for Scientific  
421 Research NWO. The authors want to thank the support of the mechanical  
422 and electronics departments at Nikhef and the detector laboratory in Bonn.  
423 The measurements leading to these results have been performed at the Test  
424 Beam Facility at DESY Hamburg (Germany), a member of the Helmholtz  
425 Association (HGF).

426 **References**

427 [1] C. Ligtenberg, et al., Performance of a GridPix detector based  
428 on the Timepix3 chip, Nucl. Instrum. Meth. A 908 (2018) 18–23.  
429 arXiv:1808.04565, doi:10.1016/j.nima.2018.08.012.

430 [2] C. Ligtenberg, et al., Performance of the GridPix detector quad,  
431 Nucl. Instrum. Meth. A 956 (2020) 163331. arXiv:2001.01540,  
432 doi:10.1016/j.nima.2019.163331.

433 [3] J. Kaminski, Y. Bilevych, K. Desch, C. Krieger, M. Lupberger, GridPix  
434 detectors - introduction and applications, Nucl. Instrum. Meth. A845  
435 (2017) 233–235. doi:10.1016/j.nima.2016.05.134.

436 [4] C. Ligtenberg, A GridPix TPC read out for the ILD experiment at the  
437 future International Linear Collider, Ph.D. thesis, Free University of  
438 Amsterdam (2021).

439 URL [https://www.nikhef.nl/pub/services/biblio/theses\\_pdf/thesis\\_C.Ligtenberg.p](https://www.nikhef.nl/pub/services/biblio/theses_pdf/thesis_C.Ligtenberg.p)

- 440 [5] M. Lupberger, Y. Bilevych, H. Blank, D. Danilov, K. Desch, A. Hamann,  
441 J. Kaminski, W. Ockenfels, J. Tomtschak, S. Zigann-Wack, To-  
442 ward the Pixel-TPC: Construction and Operation of a Large Area  
443 GridPix Detector, *IEEE Trans. Nucl. Sci.* 64 (5) (2017) 1159–1167.  
444 doi:10.1109/TNS.2017.2689244.
- 445 [6] T. Poikela, J. Plosila, T. Westerlund, M. Campbell, M. De Gaspari,  
446 X. Llopart, V. Gromov, R. Kluit, M. van Beuzekom, F. Zappone,  
447 V. Zivkovic, C. Brezina, K. Desch, Y. Fu, A. Kruth, Timepix3: a 65K  
448 channel hybrid pixel read out chip with simultaneous ToA/ToT and  
449 sparse read out, *JINST* 9 (05) (2014) C05013.  
450 URL <http://stacks.iop.org/1748-0221/9/i=05/a=C05013>
- 451 [7] J. Visser, M. van Beuzekom, H. Boterenbrood, B. van der Heijden, J. I.  
452 Muñoz, S. Kulis, B. Munneke, F. Schreuder, SPIDR: a read-out system  
453 for Medipix3 & Timepix3, *Journal of Instrumentation* 10 (12) (2015)  
454 C12028. doi:10.1088/1748-0221/10/12/C12028.
- 455 [8] B. van der Heijden, J. Visser, M. van Beuzekom, H. Boterenbrood,  
456 S. Kulis, B. Munneke, F. Schreuder, SPIDR, a general-purpose read out  
457 system for pixel ASICs, *JINST* 12 (02) (2017) C02040. doi:10.1088/1748-  
458 0221/12/02/C02040.
- 459 [9] F. Hartjes, A diffraction limited nitrogen laser for detector calibration  
460 in high energy physics, Ph.D. thesis, University of Amsterdam (1990).  
461 URL [https://www.nikhef.nl/pub/services/biblio/theses\\_pdf/thesis\\_F\\_Hartjes.pdf](https://www.nikhef.nl/pub/services/biblio/theses_pdf/thesis_F_Hartjes.pdf)
- 462 [10] R. Diener et al., The DESY II test beam facility, *Nuclear Instru-*

- 463       ments and Methods in Physics Research. Section A: Accelerators, Spec-  
464       trometers, Detectors and Associated Equipment 922 (2019) 265–286.  
465       arXiv:1807.09328, doi:10.1016/j.nima.2018.11.133.
- 466 [11] P. Baesso, D. Cussans, J. Goldstein, , Journal of Instrumentation 14 (09)  
467       (2019) P09019–P09019. arXiv:2005.00310.  
468       URL <https://doi.org/10.1088/1748-0221/14/09/p09019>
- 469 [12] D. Dannheim, K. Dort, L. Huth, D. Hynds, I. Kremastiotis, J. Kröger,  
470       M. Munker, F. Pitters, P. Schütze, S. Spannagel, T. Vanat, M. Williams,  
471       , Journal of Instrumentation 16 (03) (2021) P03008. doi:10.1088/1748-  
472       0221/16/03/p03008. arXiv:2011.12730.  
473       URL <https://doi.org/10.1088/1748-0221/16/03/p03008>
- 474 [13] R. Veenhof, Garfield - simulation of gaseous detectors, version 9, Refer-  
475       ence W5050 (1984-2010).  
476       URL <https://garfield.web.cern.ch>
- 477 [14] C. Kleinwort, General broken lines as advanced track fitting method,  
478       Nuclear Instruments and Methods in Physics Research Section A: Accel-  
479       erators, Spectrometers, Detectors and Associated Equipment 673 (2012)  
480       107–110. doi:10.1016/j.nima.2012.01.024.
- 481 [15] S. F. Biagi, Monte Carlo simulation of electron drift and diffusion  
482       in counting gases under the influence of electric and magnetic fields,  
483       Nucl. Instrum. Meth. A421 (1-2) (1999) 234–240. doi:10.1016/S0168-  
484       9002(98)01233-9.  
485       URL <https://magboltz.web.cern.ch/magboltz>